Relative Generality and Risk: Quantitative Measures For Broad Catalyst Success

Michal Sanocki,[†] Hayley Russell,[†, ‡] Jasemine Handjaya, [†] and Jolene P. Reid[†*]

[†]Department of Chemistry, University of British Columbia, Vancouver, British Columbia V6T 1Z1, Canada

ABSTRACT: The performance of chiral catalysts is typically evaluated against empirical reaction outputs like yield and selectivity with traditional analyses limited to a single model system. Expansion of the reaction space permits catalysts to be assessed for generality and this provides another useful metric for measuring the effectiveness of a catalyst. The catalyst generality algorithm will assign quantitative generality values to catalyst structures but such broad assessments are applied with the assumption that the reactions under evaluation are more or less the same by disregarding any inherent challenges associated with a particular reaction class. To address this limitation, we introduce two new metrics, relative generality and risk. These are designed to correct for variations in reaction difficulty and enable a more nuanced evaluation of catalyst performance relative to the specific demands of each reaction. We show in a number of challenging examples that these metrics allow researchers to distinguish between catalysts genuinely exhibiting superior performance and those appearing favorable due to application toward less demanding reactions. This represents a significant advancement in quantifying catalyst success, with demonstrated applications in retrospective analyses and early insights into emerging catalyst classes.

Introduction

Well performing catalyst structures are determined by a meticulous process involving the generation and analysis of experimental outcomes against multiple reaction objectives, like yield and selectivity. While these metrics allow for a straightforward assessment of catalyst function, they do not account for the difficulty in facilitating a certain class of reactions. Trained organic chemists are acutely aware of reactions that generate quaternary centers are exceptionally difficult to perform in high yields and selectivity.[1] Further, imparting enantioselectivity in reactions that require the catalyst to differentiate between near-equally sized groups is an enormous challenge.[2] Catalysts capable of effectively promoting such difficult transformations are highly prized synthetic tools enabling the synthesis of otherwise inaccessible molecules. Although the notion of reaction difficulty as a benchmark to test catalysts against is well known to practitioners, it has not yet been formalized as a criterion in catalyst assessment.

Constraining the analysis to one set of starting materials minimizes the impact that reaction difficulty will have on the final result but limits broad assessments of catalyst performance. Indeed, modern catalyst screens aim to maximize the diversity of the chemical space under evaluation to determine the catalyst's applicability.[3-4] Unintentionally, implementing this type of protocol may introduce reactions with varying degrees of difficulty, potentially obscuring the true effectiveness of certain catalysts. This overarching issue in catalyst performance assessment is often exasperated by situations where a catalyst demonstrates wide applicability but provide poor outcomes in challenging transformations, and vice versa (Figure 1). These factors, combined with the complex nature of modern reactions and the subtle variation in reaction conditions between similar substrates, can make the identification of genuinely superior catalysts challenging.[5] This raises questions: 1) Can a catalyst that overcomes the intrinsic challenges of a reaction be considered more effective than those systems that only facilitate straightforward transformations ? 2) If so, how can the difficulty of one reaction be distinguished from another? And finally 3) can this information be distilled into a single measurement for catalyst evaluation? Herein, we begin to probe these questions by developing methodologies that systematically evaluate the performance of catalysts across a diverse range of reactions, taking into account both their ability to address challenging transformations and their effectiveness in promoting straightforward ones (Figure 1). This work represents new measures of catalyst success and will prove valuable to researchers in identifying the most effective catalyst structures by providing additional context to their experimental results.

Measuring Broad Spectrum Success

Analyzing experimental selectivities collected from diverse reactions is now a well-established approach for assessing the broad applicability of a catalyst.[6-10] A powerful way for interpreting the results of these experiments is to calculate

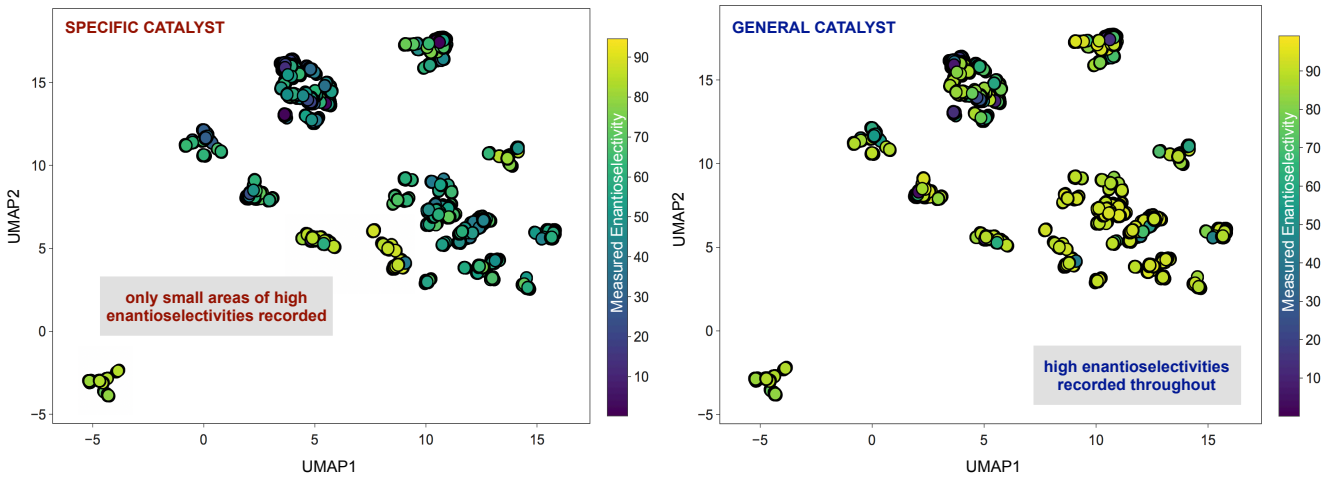

Figure 1. Theoretical comparison of a specific catalyst that works well on challenging transformations compared to a general catalyst that demonstrates good selectivities throughout. The goal of this work is to develop techniques to allow for catalysts exhibiting these characteristics to be analyzed and compared.

the catalyst generality, a measure recently introduced by our group.[11] Our algorithm assigns generality values by determining the percentage of reactions in which a catalyst surpassed a user-set threshold. Key to this approach is the implementation of non-linear dimensionality reduction and unsupervised clustering techniques to define reactions with a similar distribution of properties. This workflow offers a comprehensive evaluation of the catalyst's performance across multiple unique reactions and has proven useful in shortening the timelines for reaction optimization.[11,12] However, such extensive assessments are applied with the assumption that the reactions being evaluated are largely similar, discounting any inherent challenges associated with a particular reaction or substrate class. More specifically, because the previous approach to calculating catalyst generality relied on setting a threshold, reactions were treated uniformly. To put this into perspective, a catalyst reaching the threshold in one cluster but not in another received the same score as a catalyst performing well in the opposite situation. A second problem with our approach was that it could not distinguish between well performing catalysts. After the threshold was reached, all catalysts were treated equivalently; for instance, when a threshold of 70 % was set, catalysts achieving 80% and 90 %, were assigned the same score. Defining reaction difficulty within performative metrics becomes even more relevant for catalyst systems that demonstrate some specificity towards simple or complex reactions. Until now, in these very common situations, chemists lacked a reliable method to quantify catalyst performance across a broad spectrum of reactions with varying complexity levels.

In designing our approach, we realized that both generality and the ability to facilitate challenging reactions are valuable attributes in catalyst design and optimization, depending on the specific synthetic goals and requirements. In other words, in certain situations, a user may value the ability of a catalyst to maintain high levels of selectivity in adverse scenarios compared to broad spectrum success. Therefore, we pursued several different tactics which ultimately provide a flexible approach that permits end users to define how reaction difficulty would be weighted within the workflow (Figure 2).

Challenging reactions typically have higher enantioselectivity requirements as they often involve substrates that are less amenable to enantioinduction through simple steric control. Therefore, we considered that enantioselectivity differences between reaction types serve as a readout for reaction complexity. Basically, applying catalysts to facilitate a complex reaction would lead to lower maximum and minimum levels of enantioselectivity being recorded. On this basis, one approach could focus on correcting for reaction difficulty by applying adjustments or normalization techniques to the experimental data to account for the varying degrees of complexity among different reactions. The most straightforward method to achieve this would be to calculate the average enantioselectivity each catalyst achieves in distinct transformations and rank the results (equivalently, integrating over thresholds for the previous generality metric). By standardizing the scale for catalysts across all reactions, regardless of their actual enantioselectivity, it allows for differentiation among reactions of varying complexity (Figure 2A). This is crucial because the aim is often to select the best available option, and achieving the highest, albeit relatively low score in a difficult reaction may be more significant than attaining a relatively high score but not the highest in an easy reaction. Indeed, this approach acknowledges that some reactions inherently yield lower enantioselectivity values due to their complexity, and it evaluates catalysts based on how well they perform relative to others in those challenging scenarios.

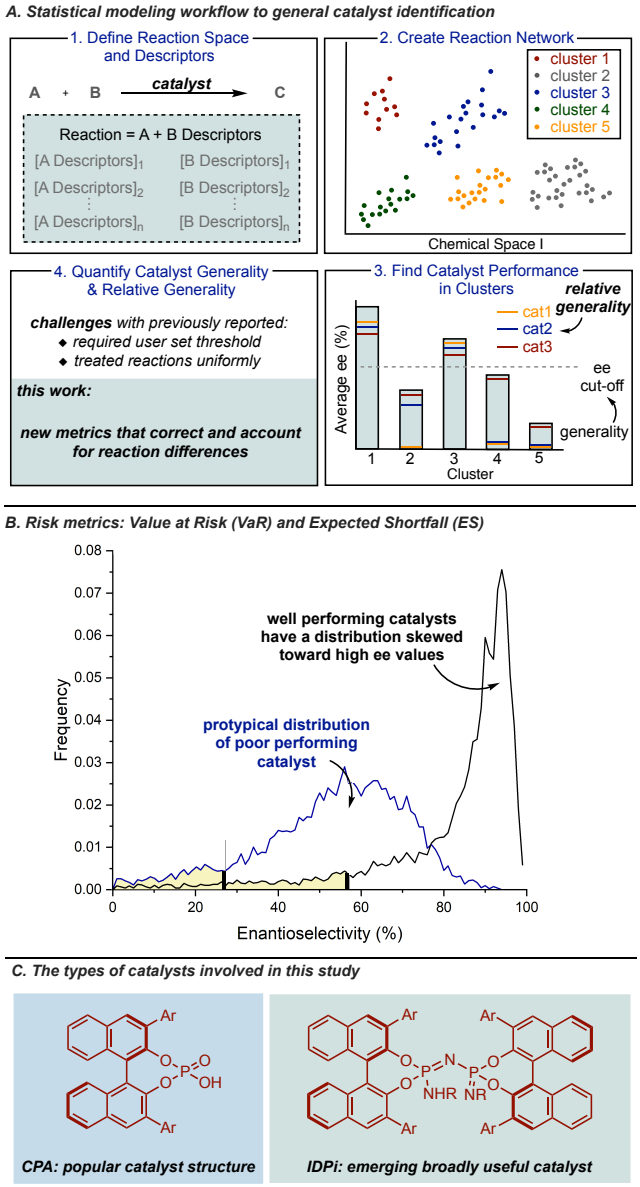

Figure 2. (A) Overview of the workflow to assign the generality and relative generality scores. Relative generality scores have been assigned to correct for reaction differences by measuring catalyst performance relative to the demands of that reaction as defined by clustering. (B) Risk metrics account for reaction differences by penalizing catalysts that perform well in straightforward transformations. Value at Risk (VaR) is shown as the bold line and Expected Shortfall (ES) is the mean of the pale yellow field. VaR and ES sample only a small part of the enantioselectivity distribution for each catalyst. (C) Chiral phosphoric acid (CPA) and imidodiphosphorimidate (IDPi) are the two catalyst classes under investigation in this study.

As this analysis now represents an extension of the applicability of the catalyst generality method, we distinguish it here by using the term 'relative catalyst generality' since it is modified to evaluate catalysts relative to the specific demands of each reaction. In this context, a catalyst ranking the most selective in one reaction receives a score of 1, while the least selective is provided with a score of 0. This scale remains consistent for all reactions, regardless of the actual enantioselectivity differences. The scores, applied on a reaction-by-reaction basis, are then averaged over all reactions within a given cluster. Therefore, this type of catalyst generality metric prioritizes catalysts that outperform others, with the best catalyst achieving an average enantioselectivity score of 1 (corresponding to the maximum in each reaction).

An entirely different technique would focus on weighting a catalyst as more effective in cases where they demonstrate resilience in challenging scenarios like those described above. To achieve this, we introduced two well established risk metrics from quantitative finance, namely Value at Risk (VaR)[13] and Expected Shortfall (ES).[14] Within this framework, a catalyst's efficiency was redefined as its ability to maintain favorable outcomes even in adverse scenarios. This approach, notably, places a strong emphasis on reactions with low enantioselectivity scores, underlining the catalyst's robustness in challenging situations (Figure 2B). However, this approach will likely minimize assessments of catalyst performance in relatively straightforward reactions. Consequently, even if a catalyst demonstrated suboptimal performance in easy reactions while excelling in difficult ones, it could still attain a high score. Essentially, VaR measures the maximum potential low enantioselectivity a catalyst might cause in a challenging reaction (usually using α = 10% of worst outcomes), while ES calculates the expected effect beyond VaR, offering insights into the catalyst's performance under difficult conditions. Figure 2B shows catalysts that are characterized by higher VaR values indicate a lower risk of undesirable reaction outcomes. This allows one not just to distinguish good catalysts from poor ones but also to provide an indication of the level of risk that can be placed in its application. As a result, this metric can be used to answer different questions to the catalyst generality measures and will provide a more comprehensive evaluation of catalyst performance, in scenarios where result disparities between easy and difficult reactions are substantial. To comprehensively assess the newly devised metrics, in this work we will challenge the measures against two different types of Brønsted acid structures (Figure 2C).

General Approach

A typical process for assessing catalyst performance starts with literature data collection, which frequently includes an unequal distribution of tested reactions across catalyst types. Owing to the influence that imbalanced datasets will have on the final result, a critical next step is to augment literature data sets with virtual data (i.e., predicted values) gathered from well validated regression models. This workflow component ensures that each catalyst's usage frequency is consistent and substantial coverage of the reaction space is attained. Consequently, throughout our analysis, we evaluate several regression models for correlating the enantioselectivity outcomes represented as $\Delta\Delta G‡$ to the structure of the reaction components. In principle, this step can be implemented with different numerical descriptors and machine learning algorithms, with the ideal choice likely dependent on the problem at hand. In this study, we mostly utilized either RDKit, quantum mechanical, and steric descriptors to efficiently transform the reaction components into numerical descriptors.[15-17] For reasons explained below, we also introduce a new descriptor set based on chemical space networks (CSN). The resulting models are

then deployed to create a virtual dataset by predicting the enantioselectivity for reported and new combinations of reactants and catalysts contained in the experimental database. Using this data, the metrics are computed, and the results ranked to determine well-performing catalyst structures.

Generality and relative generality achieves this by first revealing distinct reaction types within the virtual dataset using non-linear dimensionality reduction and unsupervised clustering. More specifically, each individual reaction is determined by a linear combination of nucleophile and electrophile properties. The reaction space expressed by these descriptors is first reduced by Uniform Manifold Approximation and Projection (UMAP)[18] followed by k-means clustering. Our motivation for including these techniques is demonstrated by the superior performance of UMAP as compared to PCA and the noted challenges in clustering high-dimensional data.[19-20] While UMAP will inherently group similar reactions together, the precise reaction boundaries can be difficult to define. Consequently, k-means is applied as a decisive clustering method, where the hyperparameter k is determined by the elbow and silhouette methods. Taking these steps together, the generality of a catalyst is described as the proportion of clusters with an average performance higher than the user set threshold. This can be formulated as:

(1)

$$generality = \frac{1}{K}\sum_{i=1}^{K}(success)_i$$

where K is the total number of clusters, and successes are defined as clusters wherein the average performance is higher than the set threshold. Relative catalyst generality removes the need for a user set threshold by considering the average enantioselectivity across all clusters, followed by normalization. This can be expressed as:

(2)

$$relative\ generality = \frac{1}{K}\sum_{i=1}^{K}(Normalized\_value)_i$$

In contrast, VaR is calculated by determining the loss value at a specified percentile of the predicted enantioselectivity distribution (shown as X) at a given significance level α. This feature removes the need for explicit reaction clusters to be defined and is calculated according to equation 3:

(3)

$$VaR_\alpha(X) = percentile_\alpha(X)$$

ES is then computed to calculate the average value of losses exceeding the VaR over the specified range of significance levels using the following equation:

(4)

$$ES_\alpha(X) = \frac{1}{1-\alpha}\int_0^\alpha VaR_u(X)du$$

Therefore, ES takes into account values lower than the VaR, potentially offering additional insight into poor performances.

Results and Discussion

Retrospective analyses. Our goal of improving the catalyst generality measurement by eliminating the dependence on user set thresholds and accounting for reaction complexity was inspired by recent results collected in our lab. Basically, as part of our experimental efforts in assessing general catalyst screening sets for retrospective optimization we attempted to improve upon an early reaction result (Scheme 1).[21] Despite applying catalyst structures now considered broadly applicable, subsequent rounds of evaluations revealed persistently low enantioselectivities, indicating potential limitations inherent to the substrate under the reaction conditions. This observation raised questions about our ability to account for variations in catalyst performance with different substrate types and prompted us to re-evaluate the chiral phosphoric acid (CPA) catalyzed nucleophilic additions to imines as a first case study. We posited this effort would deepen our mechanistic understanding of catalyst applicability across diverse reactions and enable the development of robust evaluation criteria.

Scheme 1. Attempted use of the catalyst generality scores to improve upon a previously reported reaction.[a]

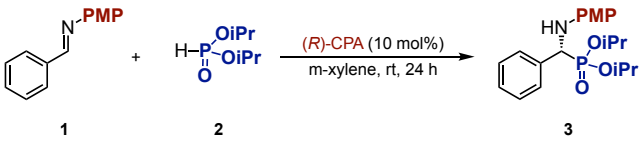

1 2 3

entry	3,3' group	Generality	Yield[c] (%)	ee[d] (%)
1	2,4,6-$(Cy)_3C_6H_2$	1.35[b]	87	13
2	2,4,6-$(iPr)_3C_6H_2$	0.92	83	24
3	9-phenanthryl	0.80	68	36
4	9-anthryl	0.78	81	15
5	3,5-$(CF_3)_2C_6H_3$	0.76	91	44
6	2,6-$(Me)_2C_6H_3$	0.74	80	21
7	1-naphthyl	0.68	24	17
8	3,5-$(NO_2)_2C_6H_3$	0.66	87	38
9	2,4,6-$(Me)_3C_6H_2$	0.66	77	21
10	3,5-$(Ph)_2C_6H_3$	0.54	67	18
11	Ph	0.24	35	19

[a]Reactions were run with the following conditions: Imine substrate (0.1 mmol), diisopropyl phosphonate (0.2 mmol), (*R*)-chiral phosphoric acid (10 mol%), anhydrous m-xylene (1 mL), rt, 24 h. [b] Catalyst generality predicted by the previously reported MLR model.[11] [c]Isolated yields given. [d]Enantioselectivities (ee) were measured by SFC. See the Supporting Information for further details.

Our previous work established that the enantioselectivity afforded by distinct reaction types can be connected through a XGBoost regression model that describes the

structure of the imine, nucleophile, and catalyst through a range of molecular features.[11] These encompassed DFT acquired structural descriptors that serve to describe the size and electronic features of the molecules through Sterimol values, IR vibrations, NBO charges, energies of molecular orbitals and polarizability. The experimental data set included a total of 364 reactions that proceed through an E(+ee) or a Z(-ee) imine transition state.[22] Differentiating between the two imine forms is important in understanding the enantioselectivity outcome, as nucleophile addition to the same face will lead to different enantiomers. Thus, the sign of the enantioselectivity value aligns with a certain imine geometry and this information can be used to predict the absolute product stereochemistry. To assemble the virtual dataset, the model was applied to predict the enantioselectivities arising from each permutation of imine, nucleophile, and catalyst contained in the experimentally curated data set (125460 reactions consisting of 15 catalysts×8,364 reactants). Following UMAP reduction to 10 dimensions, the substrate space was clustered with the k means algorithm (k = 50) and the relative generality values were determined from the virtual data for the 15 CPA catalysts (Figure 3A). As compared to generality, relative generality displayed minimal differences in catalyst ordering. TRIP is assigned as the most general catalyst, while 9-phenanthryl and 9-anthryl derived chiral phosphoric acids were predicted to be slightly less applicable. However, relative generality revealed more pronounced distinctions between high-performing catalysts and others by adjusting for variations in individual reaction performances. Catalysts typically ranking at the top received scores close to one, while those ranking lower scored closer to zero. To further interrogate the impact of reaction difficulty on broad catalyst performances, we also computed the risk metrics (Figure 3B). Inspection of this data shows one significant difference to be in the case of 9-anthryl, which ranks much lower on this scale than the previous. Interestingly, several less general catalyst structures were measured to be highly versatile, including those containing 3,5-Ph substituents. As such, we were motivated to understand these results better by decomposing the contributions of chemical space and enantioselectivity values to the catalyst scores. Figure 4 shows this data simultaneously in a line diagram, where each peak or valley represents a cluster of unique reaction space branded by the two catalysts: 9-anthryl (black line) and 3,5-Ph (blue line). While there are some substrates where 3,5-Ph is the more selective catalyst, it is clear that 9-anthryl is better for a larger range of substrates (i.e. more yellow between the two lines than grey), explaining the higher generality and relative generality scores. In a separate diagram we elected to present information gained from the risk metric, alongside the chemical space. This visualization scheme displays some of the same information contained in Figure 4, but in a manner that better facilitates the identification of relative catalyst performance differences as measured by risk. As a demonstration of this visualization technique, the enantioselectivities for the two catalysts was plotted relative to the least ranked catalyst as determined by the risk metrics, in this case, the catalyst including 4-$NO_2C_6H_4$ groups. This allows for any relative performance gains (or losses) to be linked to certain reaction types. We reasoned that in straightforward

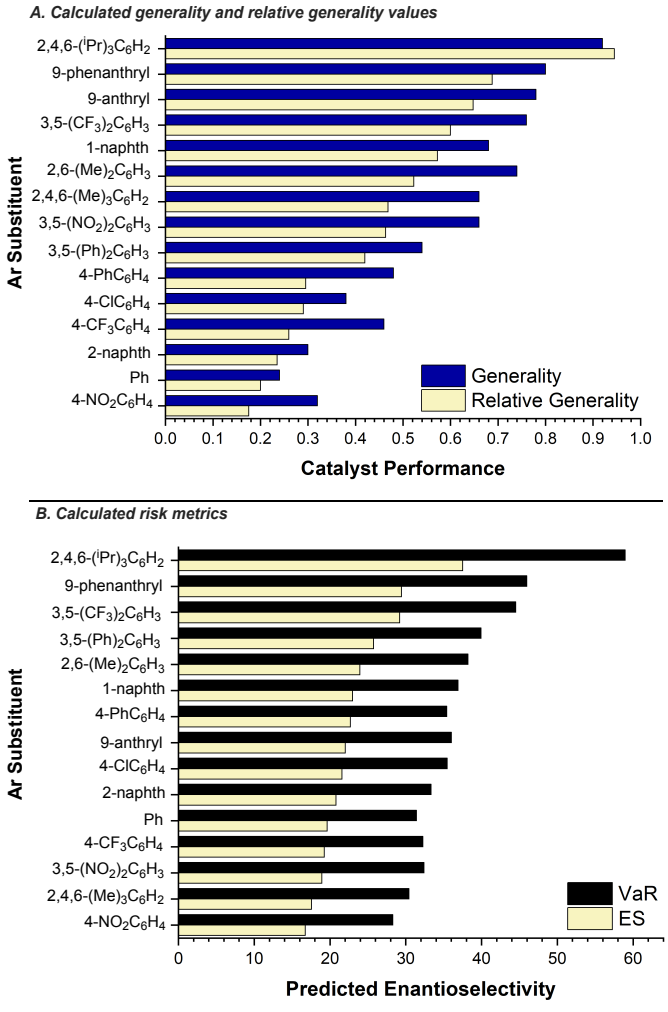

Figure 3. Obtained catalyst scores for the CPA catalyzed nucleophilic addition to imines. (A) Relative generality and (B) VaR and ES (known collectively as risk metrics).

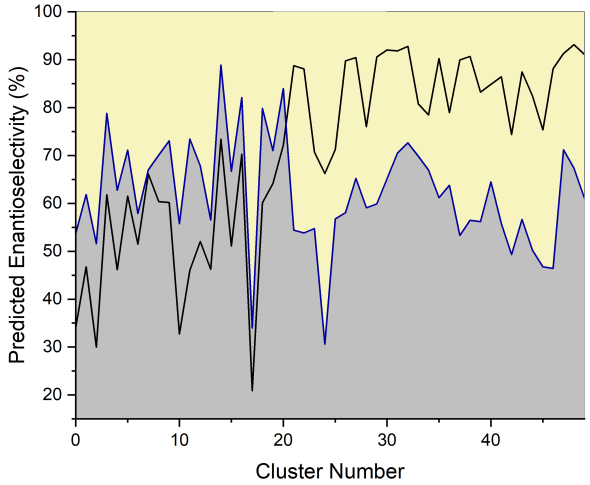

Figure 4. Predicted average performance within each cluster. 9-anthryl performances displayed by the blue line while 3,5-Ph shown in black. When the space between blue and black lines is grey, 3,5-Ph is more selective. In contrast, when the space is yellow, 9-anthryl is better.

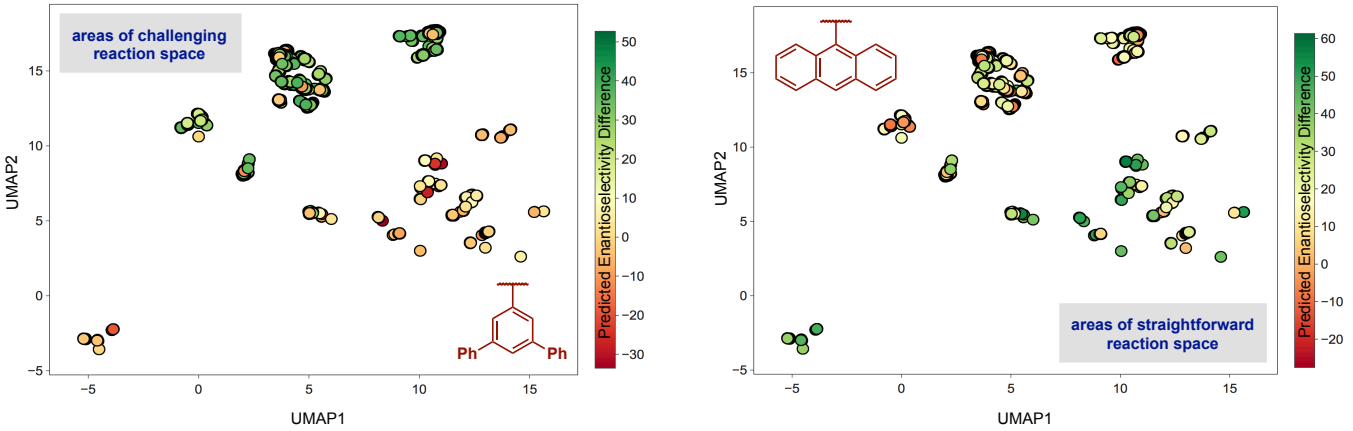

Figure 5. UMAP visualization of some of the reactions present (i.e., filtered for ee <50% measured by catalyst ranked lowest by risk). The colors indicate relative performance of 3,5-Ph and 9-anthryl compared to the baseline catalyst containing 4-$NO_2C_6H_4$ groups.

reactions the baseline catalyst will also show high enantioselectivities, thus, to make meaningful comparisons it is important to filter for difficult reactions i.e. where baseline catalyst had ee <50%. In other words, if the baseline catalyst was achieving 90% ee, the differences in catalyst performance could never be high. The results of this visualization approach are shown in Figure 5. Because both catalysts are ranked higher than a catalyst containing 4-$NO_2C_6H_4$ groups, there are more yellow/green dots (higher enantioselectivity) than red (lower enantioselectivity) on the UMAP plot. Further inspection of this data shows significant catalyst-substrate matching effects; however, 9-anthryl provides high enantioselectivities in reactions that can also be facilitated with other catalysts. This illustrates a powerful behavior of the risk metrics: if a catalyst excels in reaction space where numerous other catalysts also perform well, that catalyst will be penalized. These behaviors, as displayed in Figure 4 and Figure 5, clearly reflect the different questions risk and relative catalyst generality have been designed to answer.

Emerging Catalyst Classes. After evaluating our new metrics for assessing selectivity performance of a well-studied catalyst chemotype, we sought to test whether they can also be applied to a catalyst system for which general models for selectivity have not yet been developed. Hence, as a second case study, we evaluated this general workflow with another important class of Brønsted acids, namely, imidodiphosphorimidates (IDPis).[23-24] As compared to that of earlier catalyst designs like BINOL-derived phosphoric acids, the substituents at the 3,3' positions are usually distinctive. They display fewer similarities with previous designs, such as the absence of equivalents to TRIP or 9-anthryl, and vary structurally from one another.[25,26] These factors, combined with the current lack of in-depth understanding required for rational optimization through local structure searches, are some of the underlying reasons for why the diversity of well-performing structures reported in this area of organocatalysis is significant. Indeed, these intriguing mechanistic features are further highlighted by the observation that several structures have seen extensive use, suggesting substrate-catalyst matching. Recent reports of machine learning applied to this arena demonstrate that there are correlations to be found; however, a comprehensive model connecting multiple reaction types has yet to be established.[27] These multi-reaction models are useful for predicting the impact of new components on the enantioselectivity outcome and necessary for performing the aforementioned analysis.[28-31] Clearly, this assessment is significantly different from those previously presented, as it involves applying our developed metrics to an emerging catalyst system lacking established models for selectivity. Additionally, given the incomplete data sets, it remains uncertain whether broadly applicable catalyst structures exist yet. In the previous examples, multiple catalyst structures are analyzed under the assumption that one of these structures is the most general. This is the situation for which our metrics were designed; however, our measures could still prove useful in the event that all the catalysts display narrow applicability or several catalysts exhibit wide reaction scope.

To initiate this portion of the study, we curated a total data set of 323 reactions from 13 literature reports for parameter collection and analysis. The spread of enantioselectivity measurements is broad, comprising a ΔΔG‡ window of 2.85 kcal/mol. The training set included combinations of 37 catalysts (25 3, 3'-groups and 5 electron withdrawing groups on the nitrogen), 155 electrophiles, 49 nucleophiles, and 16 solvents. This dataset represents an intriguing body of literature and include excellent catalysts for Mukaiyama aldol,[32-33] Michael additions,[34] Diels-Alder,[8,35-38] Nazarov,[39] Prins,[40] and Hosomi-Sakurai[41] reactions. Although the general selectivity determining steps of these transformations are thought to be fundamentally similar these transformations do include structurally diverse reactants. Thus, the most significant challenge in the early stages of model building was defining suitable parameters to appropriately capture subtle differences between reaction components with limited structural overlap. The most common types of statistical modeling approaches typically utilize a breadth of structural/molecular descriptors gathered from density functional theory (DFT), quantitative structure–activity relationships (QSAR), and molecular mechanics (MM),

with the ideal choice dependent on the structures and processes being interrogated. At first, we implemented RDKit descriptors because these feature sets do not require any calculation. These 2D-descriptors are then complemented by additional features that we suspect may be absent from the simpler representation. Given the success in applying truncated molecules and DFT descriptors to define the structurally similar chiral phosphoric acid catalysts, we adopted similar techniques to build the catalyst parameter set.[42] This included computation optimizations on a truncated molecule featuring one of the 3-substituents at the M06-2X/def2-TZVP level of theory followed by collection of HOMO/LUMO, Sterimol values, %Vbur,[43] and various size/shape descriptors (see SI).[44] These types of calculations can be computationally expensive, complicated to set up, and the results are often logged manually. In cases where 100s of molecules (and their conformers) are required to be analyzed, implementing this approach would be prohibitively time-consuming. To streamline descriptor collection for the starting materials (i.e. electrophile and nucleophile), we utilized molecular mechanics minimized geometries as the parameter acquisition platform. Electrophiles encompass aldehydes, ketones, esters, and various unsaturated compounds like enones. Likewise, nucleophile structures incorporate a large range of reactive structures including silyl enol ethers, alkenes, and allyl silanes. Because the electrophile and nucleophile compounds contain the same core functionality embedded within different compound classes, we suspected that an algorithm could be developed to aid in feature extraction. Success in this effort would require formalization of reactive atoms in great detail such that a set of predefined expert-based rules could be developed. Our python application takes the SMILES strings of the candidate structures and performs a conformational search using RDKit. Upon completion, low-energy conformers are selected, and the program applies the series of carefully considered, coded rules to determine the reactive atoms present, making decisions on the important aspects of the structures. The program first matches the supplied 2D inputs against a series of rules that searches for specific atom types (C=0 and C=C bonds). Each rule encodes a structural pattern matching a certain class of electrophile or nucleophile. Based on which rule return a positive match, electrophile and nucleophile type can be determined. The rules have been coded to recognize the following variables: electrophile type (CHO or RCO) and nucleophile type depending on the location of the C=C double bond (see SI). Once assigned, it extracts the Sterimol and %Vbur values, performs Boltzmann weighting and finally stores the data for regression analysis.

Considering the proximity of the reactive centers to the catalyst structure, it is reasonable to assume these features will have a great effect on enantioselectivity outcome. However, the large size of this catalyst may allow for additional contact points further away from the reaction sites. With this in mind, we also included descriptors that represent the whole molecule structure. These include the size of the bounding box needed to encapsulate the molecule, a different type of multidimensional measure that incorporates total volume, height, and width. Likewise, information of this type could be included in a different measurement such as the distance of reacting atoms from the center of mass.

Indeed, most of the parameters surveyed are designed to distinguish one molecule from another whilst also attempting to identify appropriate parameters to connect changes in structure with enantioselectivity. The implication of these parameter types is that if similar molecules, as defined by a descriptor, all provide comparable levels of enantioselectivity, that parameter is deemed an important feature. However, a product of this approach is that local chemical neighborhoods (i.e. a measure of structural similarity) of molecules can perform similarly in many cases. On this basis and to complement these existing parameter sets, we sought to implement a descriptor set that incorporates information about the performance and characteristics of neighboring molecules into our model. To build local neighborhoods of molecules we deployed chemical space networks (CSN), a method that constructs a network consisting of nodes that correspond to molecules and edges typically representing some form of similarity index.[45-47] Crucially, networks provide an inherent representation of chemical spaces by encapsulating the discrete structure and similarity relationships among molecules without necessitating the creation of a coordinate system or dimensionality reduction. Given that similarity metrics like Tanimoto[48] and maximum common substructure (MCS),[49] can be calculated solely based on molecular structure (obtained from SMILES strings), they circumvent the challenges associated with high dimensionality observed in coordinate- and cell-based representations. Since every molecule exhibits some degree of similarity to others, a threshold must be applied to avoid a fully connected graph, making all network properties somewhat dependent on the chosen threshold. This enables the collection of experimental and local structural information that encompass the average historical performance of all neighbors of a given molecule, or the maximum and minimum average values among its neighbors. As an alternative method to capture similar behaviors across comparable structures, we incorporate one-hot encoded descriptors to differentiate between Diels-Alder reactions, addition reactions of silyl-based nucleophiles, and intermolecular transformations. Incorporating parameters to describe the solvent structure here would require significant additional descriptors and this may lead to diminished model performance (i.e., overfit). We posit that any subsequent losses in accuracy in correlating and predicting the $\Delta\Delta G^{\ddagger}$ values will affect both the training and test fits equally, and thus will not change the final conclusions sufficiently to warrant their inclusion. Finally, temperature differences were included in the Gibb's free energy equation ($\Delta\Delta G^{\ddagger} = -RT \ln|er|$) and as an independent descriptor.

With the descriptor set assembled, a machine learning model was subsequently pursued to develop a virtual data set for catalyst performance analysis and reveal the key features impacting the enantioselectivity outcome. To establish a statistically robust model, we adopted a Recursive Feature Elimination (RFE) method, which works to limit the number of variables and minimize overfitting. The algorithm works by recursively training a model on subsets of features, ranking the importance of each feature, and eliminating the least important ones. This process is repeated until a specified number of features remains or until

a predetermined performance metric is optimized. Hyperparameters for each model were tuned using random search algorithms with 10-fold cross-validation and LOO cross-validation on the optimized model. While several models were assessed in this process including Random Forest, Extra Trees, KNN Regressor, Gradient Boosting Regressor, and multivariate regression, we ultimately opted for XGBoost. This choice was motivated by its strong performance in handling complex datasets with high-dimensional features and its capacity to alleviate the problem with overfitting through regularization techniques (Figure 6). Beyond its high cross-validation and test set statistics, the model is also reasonably chemically interpretable. Specifically, the final model relies on a total of 28 descriptors, including 10 RDKit based across the three components. While these descriptors are intrinsically less information-rich than steric and neighborhood parameters they do capture the general effects that impact the reaction outcome. Selected RDKit features that are selected for the final model include, minimum and maximum partial charges, offering insights into the polarity of the molecules, along with kappa1, which indicates a degree of branching or chain-likeness. Notably, the primary catalyst features highlighted by the model pertain to the shape and size of the groups involved. This is unsurprising given their crucial role in establishing geometries conducive to asymmetric catalysis. Important descriptors include Sterimol size descriptors, min and max partial charge (RDKit), polarity, biggest distance between any two atoms, and volume of a box needed to encapsulate substituent group. The catalyst N-substituent is described only by two parameters which essentially are used to capture differences in chain length and aromaticity. Incorporating neighborhood parameters to represent the reactant structures was demonstrated to markedly enhance the accuracy of the model. Further analysis reveals a greater number of meaningful features linked to the performance of electrophiles compared to nucleophiles. This disparity may stem

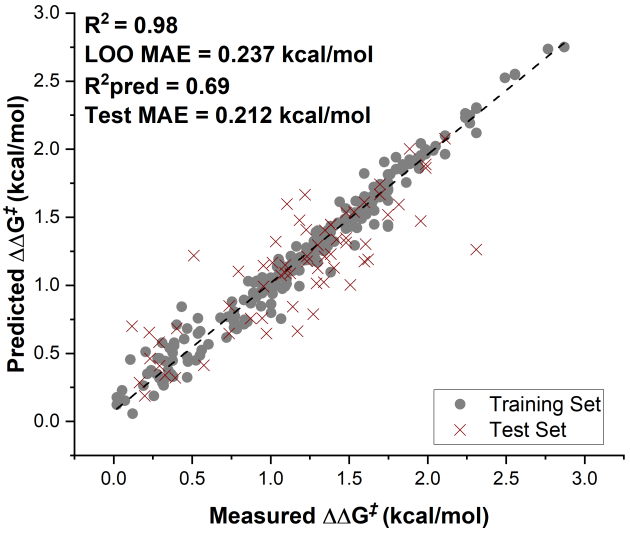

Figure 6. XGBoost model predicting the $\Delta\Delta G^{\ddagger}$ of the IDPi catalyzed addition of silyl nucleophiles to carbonyls, Diels-Alder, and intermolecular reactions (See SI for list).

from the higher variability among electrophiles (155 molecules) relative to nucleophiles (49 molecules), or potentially indicates the predominant role of electrophiles in these reactions.

The high R2pred and low test MAE demonstrate model robustness and considering that every component included in the virtual data set has in some way been represented in model training, the errors in predicting the virtual data can be expected to be similar to the training set. After careful consideration, we envisioned the safest and most meaningful virtual predictions would focus on reaction extension to include additional substrates and the screening of additional catalyst structures. To this end, the virtual dataset would be restricted to make predictions about each permutation of electrophile, nucleophile, and catalyst contained in the experimentally curated data set for particular reaction classes. In other words, all the reactants reported within Diels -Alder publications would be varied separately from published reactions involving the addition of silyl nucleophiles. Further constraints were placed on reactions that occurred intramolecularly (e.g., Nazarov) by forecasting the impact of including a new catalyst structure only. Lastly, we only considered experimentally reported catalyst structures where the N-substituent is CF_3. This was a strategic choice, to simplify the analysis and improve the accuracy of predictions by focusing only on the 3,3'-substituents.

With the virtual dataset in hand, we subsequently focused on deriving the generality, relative generality, and risk metrics. However, in questioning the proper deployment of the algorithms we were initially met with several challenges. Of these, perhaps the most important concerned the determination of the optimal threshold value, a critical parameter for computing catalyst generality. Reasoning that in an ideal ranking each catalyst should be distinguishable from another, we decided to maximize the standard deviation between catalyst performances. This feature is graphically represented in SI and allows for determining a point where increasing or decreasing the enantioselectivity threshold does not improve the variance, in this example, 90% ee. Likewise, to determine the optimal catalysts and probe the different algorithm behavior a new type of communicative visualization of the results was required given the larger number of structures and high enantioselectivities predicted for many diverse catalyst systems. Ultimately, we reasoned that in this case, the specific analysis of individual evaluation metrics are less important than insights gathered for broad substituent types. Therefore, the goal of the prediction analysis is to identify catalyst performance trends across groups of similar structures rather than distinguish between subtleties of catalyst-dependent enantioselectivity. As such, we aimed to compute each catalyst score across all metrics and summarize the data in broader catalyst bins as determined by CSN. The CSN computation essentially returned 4 catalyst groupings suggesting higher homogeneity within the catalyst structures than what was initially perceived. Structural analysis of the substituents reveals several classes of catalyst structures, varying in size. Some bins contained only 2 or 3 structures, while the two larger bins incorporated 10 or 11 catalysts. The cluster labels depended on the type of aromatic ring attached to the chiral framework (i.e., large or small) and the size and type of substituents (i.e., alkyl or perfluoroalkyl, long or short).

For example, one of these groupings contained aromatic rings with no or small substituents (i.e., Me, Et, etc.). These were grouped separately from catalysts with larger SF_5 groups and unconnected from another cluster containing structures with perfluoroalkyl chains. The final group consisted of structures with larger aromatic groups, often flat, such as pyrene-like substituents. With the structure groupings in hand for downstream analysis, we subsequently reduced the reaction space to 10 dimensions with UMAP and clustered with the k means algorithm (k = 24).

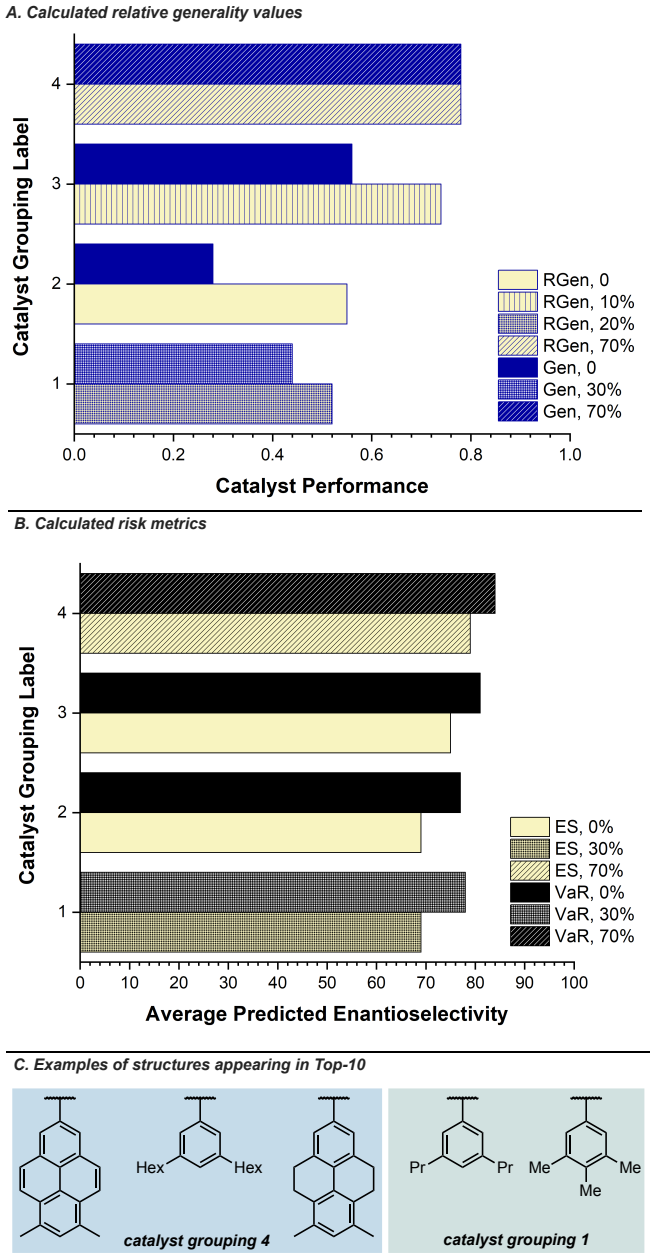

Figure 7. Summary of IDPi catalyst performances demonstrate that structures occurring in groups 4 and 1 are most useful. (A) Generality (Gen) and relative generality (RGen) values. % refers to portion of structures included in top-10. (B) Risk metrics, VaR and ES. % refers to portion of structures included in top-10. (C) Select examples of catalyst structures appearing in top-10.

The generality, relative generality, and risk values were determined from the virtual data for the 25 IDPi catalysts and the data was summarized in Figure 7. In Figure 7A and B, both the height and shading of the bars correspond to their utility. As with the previous example, larger scores indicates better catalyst performances but given how the data is summarized this can be less helpful than knowing how many of the catalyst structures are ranked within the top 10 structures. Indeed, a catalyst class that includes 70% of the top-10 structures is a better result than a catalyst class that incorporates only 30% of the structures. Figure 7A and B shows that while catalyst groups 2 and 3 generally have higher average scores for several metrics compared to catalyst group 1, the latter still contains several well-performing structures. Inspection of the individual scores (see SI), demonstrate the generality metric only identifies variance among groups of highly performing catalysts, as better catalysts tend to have a generality score close to 1, while poorer performers approach 0. In addition, several catalysts are assigned the same score resulting in a draw between different variants. Relative generality is more sensitive resulting in greater differences. This difference arises from the arbitrary threshold used in generality calculations, as the leading catalyst's score sharply declines for higher thresholds. Ultimately, suggesting that the newly reported metric can detect subtle differences in selectivity, potentially aiding decision-making, although the performance differences in this case are marginal enough to be misleading. Conversely, risk metrics produce only a slightly varied ranking of the top-10 catalysts due to their consideration of different parts of the enantiomeric excess distribution, suggesting fewer poorly performing reactions among these catalysts. Analyzing the structures of leading catalysts can also provide insights into the reasons behind the superior performance of certain IDPis. Among the top-10 returned structures of the three metrics, most appear to be relatively flat and feature large polarizable surface areas. Their large size suggests their capacity to impose strong constraints on the catalyst site, with the potential to engage in attractive noncovalent interactions. These features contribute to their high selectivity and are consistent with the findings from our statistical model. Like the earlier CPA catalyst designs, smaller groups like Ph and 2-naphthyl were poorly ranked by all metrics.

Reaction application. If we know the subsets of IDPi catalyst space that are both broadly applicability and can be applied to challenging reactions, what is the best starting point for catalyst selection? In our previous work, we demonstrated that the reaction optimization process could be streamlined by prioritizing the testing of general catalyst structures. This approach works well for examples where all of the best performing structures have been more or less reported, which is not the case for emerging catalyst structures like IDPi. However, it might be possible to leverage the information from the computations to focus local structural searches on well performing catalysts. From the standpoint of systematic exploration, the fluorene structures are ideal in that the synthesis allows for the facile preparation of potentially numerous sterically and electronically diverse derivatives from a common intermediate. In addition to synthetic accessibility and structural modularity, the fluorene catalyst substituents display molecular features important

for enantioinduction, as exemplified by their high performance metrics. Indeed, all several metrics ranked these structures all within the top-10, and two out of the three structures in the top-5 (Figure 8A). On this basis, we suspected that reaction development efforts would benefit from the deliberate application of these catalysts followed by precise structure tuning of the catalyst substituent. To test our ideas, we explored newly reported reactions where fluorene catalysts were screened (Figure 8B).[2,50-54] These reactions are not included in the model training but proceed through a mechanism similar to reactions that were used to derive the catalyst performance metrics. As such, we would also expect the catalyst trends to translate well to this system. We find that for many reported reactions fluorene-based catalysts are high performing when used, counting those structures included in our original analysis. In some cases modifications appear to be required with most focusing on altering the methylene substituents to include larger cycloalkyl groups or replacing a distal hydrogen for a larger substituent. However, the subtle changes often resulted in minor enantioselectivity improvements, indicating this optimization tactic requires an initial platform from which moderate to good selectivities can be achieved. These findings are encouraging and demonstrate how the catalyst insights could be applied to locate broadly applicable substituent platforms ripe for structure feature tuning.

A. Concept: catalyst metrics enable local structure searches

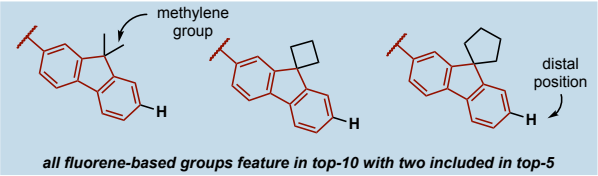

all fluorene-based groups feature in top-10 with two included in top-5

B. Validation: fluorene-based Brønsted acids are effective catalysts

Reaction description	Optimal fluorene substituent: Methylene	Optimal fluorene substituent: Distal
Desymmetrization of 4-substituted cyclohexanones		H
Addition of bis-silyl ketene acetals to a silylated aminomethyl ether		
Addition of enol silanes to an in-situ generated N-acyliminium ions		
Addition of acetic acids to an in-situ generated benzylic carbocation		
Addition of enol silanes to an in-situ generated benzylic carbocation		H
Cyanosilylation of ketones		H
Desymmetrizing silyl ether formation		H

Figure 8. Leveraging generality and risk findings for catalyst application. (A) IDPis containing fluorene substituents work broadly and in challenging cases. (B) Literature reported IDPi reactions demonstrate local structure searches in fluorene substituent space to lead to well performing catalyst structures.

Conclusion

The need for new tools to identify and quantify broadly applicable catalyst structures prompted us to develop two new measures of catalyst success, relative generality and risk. This work represents a significant step forward in catalyst performance assessment by correcting for variations in reaction difficulty**.** Our metrics include new techniques for distinguishing between straightforward and difficult reactions, allowing researchers to differentiate between catalysts that truly demonstrate superior performance and those that may seem favorable due to their application in less demanding transformations. These easily calculated metrics were rigorously evaluated in several case studies involving Brønsted acids. In each example, comparing and deconstructing the values reveals several interesting features about the basis for catalyst performance. This work also suggests how generality and risk metrics may be applied to help further guide the development of emerging catalyst classes like IDPi. Indeed, in evaluating this catalyst chemotype a multi-reaction model was pursued using traditional parameter acquisition platforms and descriptors. Here we have shown that this portion of the workflow can be accelerated by automatically extracting structural features from the text files of energy minimized structures. This data can be directly used as input for a machine learning model to predict enantioselectivities of reactions involving carbonyl-based electrophiles and structurally diverse nucleophiles. The mechanistic fidelity of the correlations was improved by incorporating information from local neighborhoods identified by CSN. Finally, we are currently integrating these approaches in ongoing projects as well as exploring the application of these metrics to reaction development.

ASSOCIATED CONTENT

Supporting Information

General workflow and model building information, database curation details, comparison of dimensionality reduction methods, experimental procedures and characterization details (PDF)

All data and code used to produce the reported results (ZIP)

AUTHOR INFORMATION

Corresponding Author

*Jolene P. Reid – Department of Chemistry, University of British Columbia, Vancouver, British Columbia V6T 1Z1, Canada. Email: jreid@chem.ubc.ca

Present Addresses

‡ Department of Pure and Applied Chemistry, University of Strathclyde, Glasgow, G1 1XL, United Kingdom

ACKNOWLEDGMENT

Financial support to J.P.R. was provided by the University of British Columbia and the Natural Sciences and Engineering Research Council of Canada (NSERC) and the CFI John R. Evans Leaders Fund. Computational resources were provided from Compute Canada and the Advanced Research Computing (ARC) center at the University of British Columbia. M.S. acknowledges Individual Travel Grant from Amsterdam University Fund. H.C.R wishes to thank the University of Strathclyde and University of Glasgow for a MacRobertson travel scholar-ship. H.C.R wishes to thank the UKRI for an iCASE studentship (EP/V519777/1).

References

(1) Quasdorf, K. W.; Overman, L. E. Catalytic enantioselective synthesis of quaternary carbon stereocentres. *Nature* **2014**, *516*, 181–191. https://doi.org/10.1038/nature14007

(2) Zhou, H.; Zhou, Y.; Bae, H. Y.; Leutzsch, M.; Li, Y. H.; De, C. K.; Cheng, G.-J.; List, B. Organocatalytic stereoselective cyanosilylation of small ketones. *Nature* **2022**, *605*, 84−89. https://doi.org/10.1038/s41586-022-04531-5

(3) Kozlowski, M. C. On the Topic of Substrate Scope. *Org. Lett.* **2022**, *24*, 7247–7249. https://doi.org/10.1021/acs.orglett.2c03246.

(4) Gensch, T.; Glorius, F. The Straight Dope on the Scope of Chemical Reactions. *Science* **2016**, *352*, 294–295. https://doi.org/10.1126/science.aaf3539.

(5) Betinol, I. O.; Reid, J. P. A predictive and mechanistic statistical modelling workflow for improving decision making in organic synthesis and catalysis. *Org. Biomol. Chem.*, **2022**, *20*, 6012-6018. https://doi.org/10.1039/D2OB00272H

(6) Prieto Kullmer, C. N.; Kautzky, J. A.; Krska, S. W.; Nowak, T.; Dreher, S. D.; MacMillan, D. W. C. Accelerating Reaction Generality and Mechanistic Insight through Additive Mapping. *Science* **2022**, *376*, 532–539. https://doi.org/10.1126/science.abn1885.

(7) Wagen, C. C.; McMinn, S. E.; Kwan, E. E.; Jacobsen, E. N. Screening for Generality in Asymmetric Catalysis. *Nature* **2022**. https://doi.org/10.1038/s41586-022-05263-2.

(8) Kim, H.; Gerosa, G.; Aronow, J.; Kasaplar, P.; Ouyang, J.; Lingnau, J. B.; Guerry, P.; Farès, C.; List, B. A Multi-Substrate Screening Approach for the Identification of a Broadly Applicable Diels–Alder Catalyst. *Nat. Commun.* **2019**, *10* (1), 770. https://doi.org/10.1038/s41467-019-08374-z.

(9) Rose, B. T.; Timmerman, J. C.; Bawel, S. A.; Chin, S.; Zhang, H.; Denmark, S. E. High-Level Data Fusion Enables the Chemoinformatically Guided Discovery of Chiral Disulfonimide Catalysts for Atropselective Iodination of 2-Amino-6-Arylpyridines. *J. Am. Chem. Soc.* **2022**, *144* (50), 22950–22964. https://doi.org/10.1021/jacs.2c08820.

(10) Rein, J.; Rozema, S. D.; Langner, O. C.; Zacate, S. B.; Hardy, M. A.; Siu, J. C.; Mercado, B. Q.; Sigman, M. S.; Miller, S. J.; Lin, S. Generality-Oriented Optimization of Enantioselective Aminoxyl Radical Catalysis. *Science* **2023**, *380*, 706– 712, https://doi.org/10.1126/science.adf6177

(11) Betinol, I. O.; Lai, J.; Thakur, S.; Reid, J. P. A Data-Driven Workflow for Assigning and Predicting Generality in Asymmetric Catalysis. *J. Am. Chem. Soc.* **2023**, *145*, 12870, https://doi.org/10.1021/jacs.3c03989

(12) Deng, Z.; Padalino, M. A.; Jan, J. E. L.; Park, S.; Dannerman, M. W.; Johnston, J. N. Generality-Driven Catalyst Development: A Universal Catalyst for Enantioselective Nitroalkene Reduction. *J. Am. Chem. Soc.* **2024**, *146*, 1269–1275. https://pubs.acs.org/doi/10.1021/jacs.3c12436

(13) Jorion, P. (2006). Value at Risk: The New Benchmark for Managing Financial Risk (3rd ed.). McGraw-Hill. ISBN 978-0-07-146495-6.

(14) Acerbi, C.; Tasche, D. Expected Shortfall: a natural coherent alternative to Value at Risk. *Economic Notes.* **2002** *31* (2): 379–388. arXiv:cond-mat/0105191. doi:10.1111/1468-0300.00091. S2CID 10772757.

(15) Santiago, C. B.; Guo, J.-Y.; Sigman, M. S. Predictive and Mechanistic Multivariate Linear Regression Models for Reaction Development. *Chem. Sci.* **2018**, *9*, 2398–2412. DOI: 10.1039/C7SC04679K

(16) Durand, D. J.; Fey, N. Computational Ligand Descriptors for Catalyst Design. Chem. Rev. 2019, 119, 6561–6594, DOI: 10.1021/acs.chemrev.8b00588

(17) Gallegos, L. C.; Luchini, G.; St. John, P. C.; Kim, S.; Paton, R. S. Importance of Engineered and Learned Molecular Representations in Predicting Organic Reactivity, Selectivity, and Chemical Properties. *Acc. Chem. Res.* **2021**, *54*, 827– 836, DOI: 10.1021/acs.accounts.0c00745

(18) McInnes, L.; Healy, J.; Melville, J. UMAP: Uniform Manifold Approximation and Projection for Dimension Reduction. *arXiv* **2020**. https://doi.org/10.48550/arXiv.1802.03426.

(19) Steinbach, M.; Ertöz, L.; Kumar, V. The Challenges of Clustering High Dimensional Data. In *New Directions in Statistical Physics*; Wille, L. T., Ed.; Springer Berlin Heidelberg: Berlin, Heidelberg, 2004; pp 273–309. https://doi.org/10.1007/978-3-662-08968-2_16.

(20) Allaoui, M.; Kherfi, M. L.; Cheriet, A. Considerably Improving Clustering Algorithms Using UMAP Dimensionality Reduction Technique: A Comparative Study. In *Image and Signal Processing*; El Moataz, A., Mammass, D., Mansouri, A., Nouboud, F., Eds.; Lecture Notes in Computer Science; Springer International Publishing: Cham, 2020; Vol. 12119, pp 317–325. https://doi.org/10.1007/978-3-030-51935-3_34.
(21) Akiyama, T.; Morita, H.; Itoh, J.; Fuchibe, K. Chiral Brønsted Acid Catalyzed Enantioselective Hydrophosphonylation of Imines: Asymmetric Synthesis of α-Amino Phosphonates. *Org. Lett*. **2005**, *7*, 2583– 2585. https://doi.org/10.1021/ol050695e
(22) Reid, J. P.; Sigman, M. S. Holistic Prediction of Enantioselectivity in Asymmetric Catalysis. *Nature* **2019**, *571*, 343–348. https://doi.org/10.1038/s41586-019-1384-z.
(23) Schreyer, L.; Properzi, R.; List, B. IDPi Catalysis. *Angew. Chem., Int. Ed.* **2019**, *58*, 12761– 12777. https://doi.org/10.1002/anie.201900932
(24) Cheng, J. K.; Xiang, S.-H.; Tan, B. Imidodiphosphorimidates (IDPis): Catalyst Motifs with Unprecedented Reactivity and Selectivity. *Chin. J. Chem.* **2023**, *41*, 685–694. https://doi.org/10.1002/cjoc.202200618
(25) Lai, J.; Reid, J. P. A Bulky Imidodiphosphorimidate Brønsted Acid Enables Highly Enantioselective Prins-semipinacol Rearrangements. *ChemRxiv* **2022**, DOI: 10.26434/chemrxiv-2023-w1s3m-v2 April242024Accessed
(26) Schwengers, S. A.; De, C. K.; Grossmann, O.; Grimm, J. A. A.; Sadlowski, N. R.; Gerosa, G. G.; List, B. Unified Approach to Imidodiphosphate-Type Brønsted Acids with Tunable Confinement and Acidity. *J. Am. Chem. Soc.* **2021**, *143*, 14835-14844 https://doi.org/10.1021/jacs.1c07067
(27) Tsuji, N.; Sidorov, P.; Zhu, C.; Nagata, Y.; Gimadiev, T.; Varnek, A.; List, B. Predicting Highly Enantioselective Catalysts Using Tunable Fragment Descriptors. *Angew. Chem., Int. Ed.* **2023**, *62*, e202218659 https://doi.org/10.1002/anie.202218659
(28) Shoja, A.; Reid, J. P. Computational Insights into Privileged Stereocontrolling Interactions Involving Chiral Phosphates and Iminium Intermediates. *J. Am. Chem. Soc.* **2021**, *143*, 7209–7215. https://doi.org/10.1021/jacs.1c03829
(29) Shoja, A.; Zhai, J.; Reid, J. P. Comprehensive Stereochemical Models for Selectivity Prediction in Diverse Chiral Phosphate-Catalyzed Reaction Space. *ACS Catal.* **2021**, *11*, 11897-11905. https://doi.org/10.1021/acscatal.1c03520
(30) Lai, J.; Reid, J. P. Interrogating the thionium hydrogen bond as a noncovalent stereocontrolling interaction in chiral phosphate catalysis. *Chem. Sci*. **2022**, *13*, 11065-11073. https://doi.org/10.1039/D2SC02171D
(31) Kuang, Y.; Lai, J.; Reid, J. P. Transferrable selectivity profiles enable prediction in synergistic catalyst space. *Chem. Sci.* **2023**, *14*, 1885-1895. https://doi.org/10.1039/D2SC05974F
(32) Bae, H. Y.; Höfler, D.; Kaib, P. S. J.; Kasaplar, P.; De, C. K.; Döhring, A.; Lee, S.; Kaupmees, K.; Leito, I.; List, B. Approaching sub-ppm-level asymmetric organocatalysis of a highly challenging and scalable carbon–carbon bond forming reaction. *Nat. Chem.* **2018**, *10*, 888– 894, DOI: 10.1038/s41557-018-0065-0
(33) Schreyer, L.; Kaib, P. S. J.; Wakchaure, V. N.; Obradors, C.; Properzi, R.; Lee, S.; List, B. Confined acids catalyze asymmetric single aldolizations of acetaldehyde enolates. *Science* **2018**, *362*, 216– 219, DOI: 10.1126/science.aau0817
(34) Gatzenmeier, T.; Kaib, P. S.; Lingnau, J. B.; Goddard, R.; List, B. The Catalytic Asymmetric Mukaiyama– Michael Reaction of Silyl Ketene Acetals with α, β-Unsaturated Methyl Esters. *Angew. Chem., Int. Ed.* **2018**, *57*, 2464– 2468, DOI: 10.1002/anie.201712088
(35) Liu, Lu.; Kim, H.; Xie, Y.; Farès, C.; Kaib, P. S. J.; Goddard, R.; List, B. Catalytic Asymmetric [4+2]-Cycloaddition of Dienes with Aldehydes. *J. Am. Chem. Soc.* **2017**, *139*, 13656-13659, DOI: 10.1021/jacs.7b08357
(36) Ghosh, S.; Das, S.; De, C. K.; Yepes, D.; Neese, F.; Bistoni, G.; Leutzsch, M.; List, B. Strong and Confined Acids Control Five Stereogenic Centers in Catalytic Asymmetric Diels–Alder Reactions of Cyclohexadienones with Cyclopentadiene. *Angew. Chem., Int. Ed.* **2020**, *59*, 12347–12351, DOI: 10.1002/anie.202000307
(37) Ghosh, S.; Erchinger, J. E.; Maji, R.; List, B. Catalytic Asymmetric Spirocyclizing Diels-Alder Reactions of Enones: Stereoselective Total and Formal Syntheses of α-Chamigrene, β-Chamigrene, Laurencenone C, Colletoic Acid, and Omphalic Acid. *J. Am. Chem. Soc.* **2022**, *144*, 6703– 6708, DOI: 10.1021/jacs.2c01971
(38) Gatzenmeier, T.; Turberg, M.; Yepes, D.; Xie, Y.; Neese, F.; Bistoni, G.; List, B. Scalable and Highly Diastereo-and Enantioselective Catalytic Diels-Alder Reaction of α, β-Unsaturated Methyl Esters. *J. Am. Chem. Soc.* **2018**, *140*, 12671– 12676, DOI: 10.1021/jacs.8b07092
(39) Ouyang, J.; Kennemur, J. L.; De, C. K.; Farès, C.; List, B. Strong and Confined Acids Enable a Catalytic Asymmetric Nazarov Cyclization of Simple Divinyl Ketones. *J. Am. Chem. Soc.* **2019**, *141*, 3414– 3418, DOI: 10.1021/jacs.8b13899
(40) Xie, Y.; Cheng, G. J.; Lee, S.; Kaib, P. S. J.; Thiel, W.; List, B. Catalytic Asymmetric Vinylogous Prins Cyclization: A Highly Diastereo- and Enantioselective Entry to Tetrahydrofurans. *J. Am. Chem. Soc.* **2016**, *138*, 14538– 14541, DOI: 10.1021/jacs.6b09129
(41) Kaib, P. S.; Schreyer, L.; Lee, S.; Properzi, R.; List, B. Extremely active organocatalysts enable a highly enantioselective addition of allyltrimethylsilane to aldehydes. *Angew. Chem., Int. Ed.* **2016**, *55,* 13200– 13203, DOI: 10.1002/anie.201607828
(42) Reid J. P.; Proctor R. S. J.; Sigman M. S.; Phipps R. J. Predictive Multivariate Linear Regression Analysis Guides Successful Catalytic Enantioselective Minisci Reactions of Diazines. *J. Am. Chem. Soc.* **2019**, *141*, 19178–19185. 10.1021/jacs.9b11658.
(43) Gómez-Suárez, A.; Nelson, D. J.; Nolan, S. P. Quantifying and Understanding the Steric Properties of N-Heterocyclic Carbenes. *Chem. Commun.* **2017**, *53*, 2650– 2660, DOI: 10.1039/c7cc00255f

(44) Brethomé, A. V.; Fletcher, S. P.; Paton, R. S. Conformational Effects on Physical-Organic Descriptors: The Case of Sterimol Steric Parameters. *ACS Catal.* **2019**, *9*, 2313–2323. https://doi.org/10.1021/acscatal.8b04043.

(46) Scalfani, V. F.; Patel, V. D.; Fernandez, A. M. Visualizing chemical space networks with RDKit and NetworkX. *J Cheminform*, **2022,** *14*, 87. https://doi.org/10.1186/s13321-022-00664-x.

(47) Perrone, G.; Unpingco, J.; Lu, H.-M. Network visualizations with Pyvis and VisJS. *arXiv* **2020**. https://arxiv.org/abs/ 2006.04951.

(48) Holliday, J. D.; Hu, C.-Y.; Willett, P. Grouping of coefficients for the calculation of inter-molecular similarity and dissimilarity using 2D fragment Bit-strings. *Comb Chem High Throughput Screen.* **2002**, *5*, 155–166. doi: 10.2174/1386207024607338.

(49) Zhang, B.; Vogt, M.; Maggiora, G. M.; Bajorath, J. Design of chemical space networks using a Tanimoto similarity variant based upon maximum common substructures. *J. Comput. Aided Mol. Des*., **2015**, *29*, 937–950. https://doi.org/10.1007/s10822-015-9872-1

(50) Zhou, H.; Bae, H. Y.; Leutzsch, M.; Kennemur, J. L.; Bécart, D.; List, B. The Silicon-Hydrogen Exchange Reaction: A Catalytic σ-Bond Metathesis Approach to the Enantioselective Synthesis of Enol Silanes. *J. Am. Chem. Soc.* **2020**, *142*, 13695–13700, DOI: 10.1021/jacs.0c06677

(51) Zhu, C.; Mandrelli, F.; Zhou, H.; Maji, R.; List, B. Catalytic Asymmetric Synthesis of Unprotected β^2-Amino Acids. *J. Am. Chem. Soc.* **2021**, *143*, 3312–3317, DOI: 10.1021/jacs.1c00249

(52) Grossmann, O.; Maji, R.; Aukland, M. H.; Lee, S.; List, B. Catalytic Asymmetric Additions of Enol Silanes to In Situ Generated Cyclic, Aliphatic *N*-Acyliminium Ions. *Angew. Chem., Int. Ed.* **2022**, *61*, e202115036, DOI: 10.1002/anie.202115036

(53) Singh, V. K.; Zhu, C.; Kanta De, C.; Leutzsch, M.; Baldinelli, L.; Mitra, R.; Bistoni, G.; List, B. Taming secondary benzylic cations in catalytic asymmetric S N 1 reactions. *Science* **2023**, *382*, 325-329. https://doi.org/10.1126/science.adj7007

(54) Zhou, H.; Han, J. T.; Nöthling, N.; Lindner, M. M.; Jenniches, J.; Kühn, C.; Tsuji, N.; Zhang, L.; List, B. Organocatalytic Asymmetric Synthesis of Si-Stereogenic Silyl Ethers. *J. Am. Chem. Soc.* **2022**, *144*, 10156– 10161, DOI: 10.1021/jacs.2c04261